Measurement 187 (2022) 110359

Contents lists available at ScienceDirect

Measurement

journal homepage: www.elsevier.com/locate/measurement

A real-time response relative humidity sensor based on a loop microfiber coated with polyvinyl alcohol film

Dandan Sun [a,*], Jiguang Chen [a], Yongming Fu [a], Jie Ma [a,b,*]

[a] School of Physics and Electronic Engineering, Shanxi University, Taiyuan 030006, China
[b] Laser Spectroscopy Laboratory and Collaborative Innovation Center of Extreme Optics, Shanxi University, Taiyuan 030006, China

ARTICLE INFO

Keywords:
Loop microfiber interferometer
Polyvinyl alcohol (PVA)
Relative humidity (RH) sensor
Good stability

ABSTRACT

A high sensitivity optical fiber loop-based relative humidity (RH) sensor coated with polyvinyl alcohol (PVA) film is demonstrated, which has low-temperature sensitivity. The loop region of the sensor (micron-sized diameter) is very sensitive to the environmental medium due to strong evanescent fields out of fiber cladding. The refractive index (RI) sensitivity is as high as 2979 nm/RIU, while the temperature sensitivity is relatively low at 0.0075 nm/°C. The experimental results show that the sensor has the RH sensitivity of 0.533 nm/%RH (wavelength modulation) and −0.213 dBm/%RH (intensity modulation). The proposed sensor has good real-time, stability and repeatability, which provides a guarantee for accurate RH measurement.

1. Introduction

Relative humidity (RH) is an important part of environmental monitoring, which is widely used in agricultural production, atmospheric environment, food safety, archives management, electronic products production, civil engineering, and human respiration monitoring, etc. [1–6]. In recent years, many explorations and researches in RH sensing have been reported. Conventional RH sensors mainly use resistive and capacitive electronic sensors [7–10]. Some sensors have such problems as low sensitivity, complex fabrication process, large volume, weak corrosion resistance ability, and poor anti-electromagnetic interference ability, which aren't appropriate for working in magnetic fields of industrial manufacturing and magnetic resonance imaging systems.

Optical fiber sensors have attracted much attention due to miniaturization, lightweight, corrosion resistance, and anti-electromagnetic interference [11–13]. To further improve the sensitivity of fiber sensors, it is widely discussed that different RH-sensitive media are applied to various optical structures. Oliveira R et al. have proposed a dual-fiber sensor composed of a Fabry-Perot cavity based on NOA78 adhesive and a polymer fiber Bragg grating for simultaneous detection of humidity and temperature [14]. Chen G Y et al. have presented an optical hygrometer coating polyelectrolyte on multimode fiber with the sensitivity of 0.14 dB/%RH [15]. Sun D et al. have proposed that the twisted microfiber can eliminate the cross-sensitivity effect of temperature while measuring RH and the sensitivity is 121.6 pm/%RH between 46 % and 72 % [16]. Zain H A et al. have reported a zinc oxide nanorods coated microfiber loop resonator for the RH sensing with the sensitivity of 0.2774 dBm/%RH [17]. Yin B et al. have reported a uniform fiber Bragg grating and a polyvinyl alcohol (PVA) film-coated long-period grating for detecting the RH and temperature [18]. Maciak E et al. have made a low-coherence interferometric fiber optic sensor for humidity monitoring based on Nafion® thin film [19]. Among them, the microfiber has the characteristics of relatively low cost, strong evanescent field, low loss, and strong flexibility, which provides a feasible way for exploring more efficient and economical RH sensing applications.

As a kind of RH sensitive material, PVA is a water-soluble polymer, which is characterized by good compactness, high crystallinity, strong adhesion, flexible and smooth film, oil resistance, solvent resistance, and good gas permeability. This material used by sensors is non-toxic and environmentally friendly, so it can be applied in food processing, environmental monitoring, and clinical medicine on a large scale with bright prospects. Penza M et al. have described a high sensitivity surface acoustic wave sensor system for RH detection using chemically interactive PVA film [20]. Ainhoa G et al. have proposed an optical fiber RH sensor with PVA film covered on a single-mode side-polished fiber [21]. Yan G et al. have designed knob integrated fiber Bragg grating with PVA film for simultaneous measurement of RH and temperature [22]. Yeo J et al. have compared three kinds of polymer-coated microfiber sensors and found that PVA has the best humidity sensing performance [23].

* Corresponding authors.
E-mail addresses: sundd@sxu.edu.cn (D. Sun), mj@sxu.edu.cn (J. Ma).

https://doi.org/10.1016/j.measurement.2021.110359
Received 3 June 2021; Received in revised form 7 October 2021; Accepted 17 October 2021
Available online 23 October 2021

Cheng Q H et al. have proposed a tapered coreless fiber and a graphene oxide coated fiber Bragg grating for humidity measurement with a sensitivity of 143.27 pm/%RH [24]. Lin H et al. have proposed a femtosecond laser-induced spiral micro-structured single mode-multimode-single mode fiber structure coated with PVA film for detecting RH and the sensitivity is 650 pm/%RH from 35% to 70 %RH [25]. Zebian H Y et al. have proposed the RH sensor based on a no-core multimode interferometer coated with Al_2O_3-PVA composite films with a sensitivity of 0.587 nm/%RH [26]. Chen N et al. have demonstrated a high sensitivity humidity sensor with low-temperature sensitivity coated with PVA, which has a high humidity sensitivity of 0.1194 nm/%RH [27]. Most of these sensors have low sensitivity or a complex fabrication process, so it is necessary to find a kind of RH sensor with high sensitivity and simple fabrication.

In this paper, we demonstrate the RH sensor that combines the loop fiber with PVA coating to realize a high RH sensitivity and a low-temperature sensitivity. After tapering, the optical fiber forms a loop structure under the combined action of torsional force, electrostatic force, and van der Waals force. The refractive index (RI) sensitivity is up to 2979 nm/RIU and the temperature sensitivity is as low as 0.0075 nm/°C, which indicates that the loop structure has a high refractive index sensitivity and low-temperature cross response. PVA coating with fiber surface forming a uniform and stable film by the dip-coating method. The experimental results show that in the range of 40–76 %RH, the sensitivity of this sensor is as high as 0.533 nm/%RH and −0.213 dBm/%RH, with a response time of 1.8 s and a recovery time of 4 s. The proposed device exhibits excellent stability, durability against electromagnetic interference, flexibility, and miniaturization required by next-generation technologies for RH monitoring.

2. Sensing principle

Considering the symmetrical structure of the uniformly tapered cylindrical fiber, the coupling of different HE_{1n} local modes is mainly concentrated at the loop intersection. The coupling of the HE_{11} fundamental mode and the HE_{12} high-order mode is significantly stronger than other high-order modes [28]. When the length of the loop microfiber sensor structure or the refractive index change of the medium, the interference wavelength shifts. Wavelength change can be expressed as [29]:

$$\delta\lambda = \lambda\cdot\frac{1}{\Gamma}\cdot\left(\frac{\delta L}{L}+\frac{\delta(\Delta n)}{\Delta n}\right) \tag{1}$$

where δL is the variation of loop length, the length of L microring, Δn is the effective refractive index difference between the HE_{11} mode and the HE_{12} mode, and λ is the detecting wavelength. Γ is the dispersion factor: $\Gamma = 1-\frac{\lambda}{\Delta n}\frac{d\Delta n}{d\lambda}$. This value of microfiber is generally negative. In our experiments, due to the very stable structure of micro-loops, δL can be neglected, so the Eq. (1) can be simplified to:

$$\delta\lambda = \lambda\cdot\frac{1}{\Gamma}\cdot\frac{\delta(\Delta n)}{\Delta n} \tag{2}$$

Normally, the external RI sensitivity can be expressed as [28]:

$$\frac{d\lambda}{dn_{med}} = \lambda\cdot\frac{1}{\Gamma}\cdot\left(\frac{1}{\Delta n}\frac{d\Delta n}{dn_{med}}\right) \tag{3}$$

A slight change under different RH external circumstances will cause the sensor's interference fringes to drift. RH sensitivity can be expressed as [30]:

$$\frac{d\lambda}{dRH} = \lambda\cdot\frac{1}{\Gamma}\cdot\left(\frac{1}{\Delta n}\frac{d\Delta n}{dn_{med}}\frac{dn_{med}}{dRH}\right) \tag{4}$$

where n_{med} represents the refractive index of the medium.

The sensing mechanism is based on the refractive index change of medium molecules. In this paper, the optical fiber sensing part is mainly composed of the tapered fiber structure and the PVA film attached to its surface. Based on the Lorentz-Lorenz formula, the refractive index R of the medium molecules (R means the sum of the constituent ions' polarization degree) can be expressed as [31]

$$R = \frac{n_{med}^2-1}{n_{med}^2+2}\frac{M}{\rho} = \frac{4\pi}{3}N_A\gamma \tag{5}$$

where n_{med} is the refractive index of the medium. M is the medium molecular weight of the medium. ρ is the medium density. N_A is Avogadro constant, and γ is the medium polarization index. According to Eq. (5), we can get the function expression of n_{med} as follows:

$$\frac{n_{med}^2-1}{n_{med}^2+2} = \frac{4\pi\rho N_A\gamma}{3M} \tag{6}$$

We assume that the left side of the expression of Eq. (6) is N. So, Eq. (7) transformation can be expressed as:

$$N = \frac{n_{med}^2-1}{n_{med}^2+2} \tag{7}$$

Further solving the Eq. (7) to get the n_{med} expression as follows:

$$n_{med}^2 = \frac{1+2N}{1-N} \tag{8}$$

From the above equation, we can get that the refractive index changes can be related to medium density. Under assuming other factors remain unchanged if the medium shrunk after absorbing water, the density ρ increases leading to an increase in the refractive index n_{med}. But perhaps it is the reverse that the medium swelled after absorbing water to cause the density ρ decreases, which ultimately affect the index of refraction [32]. Combining Eq. (4) and (8), when the refractive index of PVA coating changes after absorbing water in different RH conditions, Δn_{med} will change with the increase of external RH, then the interference spectrum shifts continuously.

3. Experimental results and discussion

3.1. Experimental setup and fabrication of optical microfiber

In Fig. 1(a), the experimental apparatus includes a light source (amplified spontaneous emission, ASE) in the spectral range of 1528–1603 nm, a spectral analyzer (OSA, Anritsu MS9740A) to record the transmission spectrum with a wavelength resolution of 0.03 nm. The humidity environment in the chamber is generated by the humidifier. The chamber placement of a commercial electronic hygrometer displays an approximate RH value with a humidity resolution of 1% RH. The temperature is kept at about 25 °C. The moisture circumstance is adjusted and controlled in time by a micro fan. The micro fan is used to quickly adjust and control the moisture circumstance to achieve balance [33,34].

The loop humidity sensor comprises a central uniform waist area in the loop part and a tapered area on both sides. Fig. 1(b) shows the manufacturing steps of the RH sensor. An oxyhydrogen generator or a butane flamethrower is used as the high-temperature heat source with 1700–2000 °C and flame width of about 2 mm. When tapering the fiber, the heat source remains fixed (not moving), and the two stepper motors with the original fiber at both ends move in the same direction along with the fiber at different speeds under the precise control of the computer accuracy of 1 μm. Hence, the microfiber is produced successfully through automation [28], as shown in Fig. 1 (b, left top) and the corresponding spectral diagram is shown in Fig. 1 (b, right black). The microfiber includes the transition region (length of 5 mm), and the middle uniform region of 10.29 μm in diameter and 15 mm in length. We need to make a trade-off between refractive index sensitivity and transmission loss [35]. Therefore, we choose a diameter of about 10 μm. Then, the ends of the microfiber after tapering are fixed on two fiber

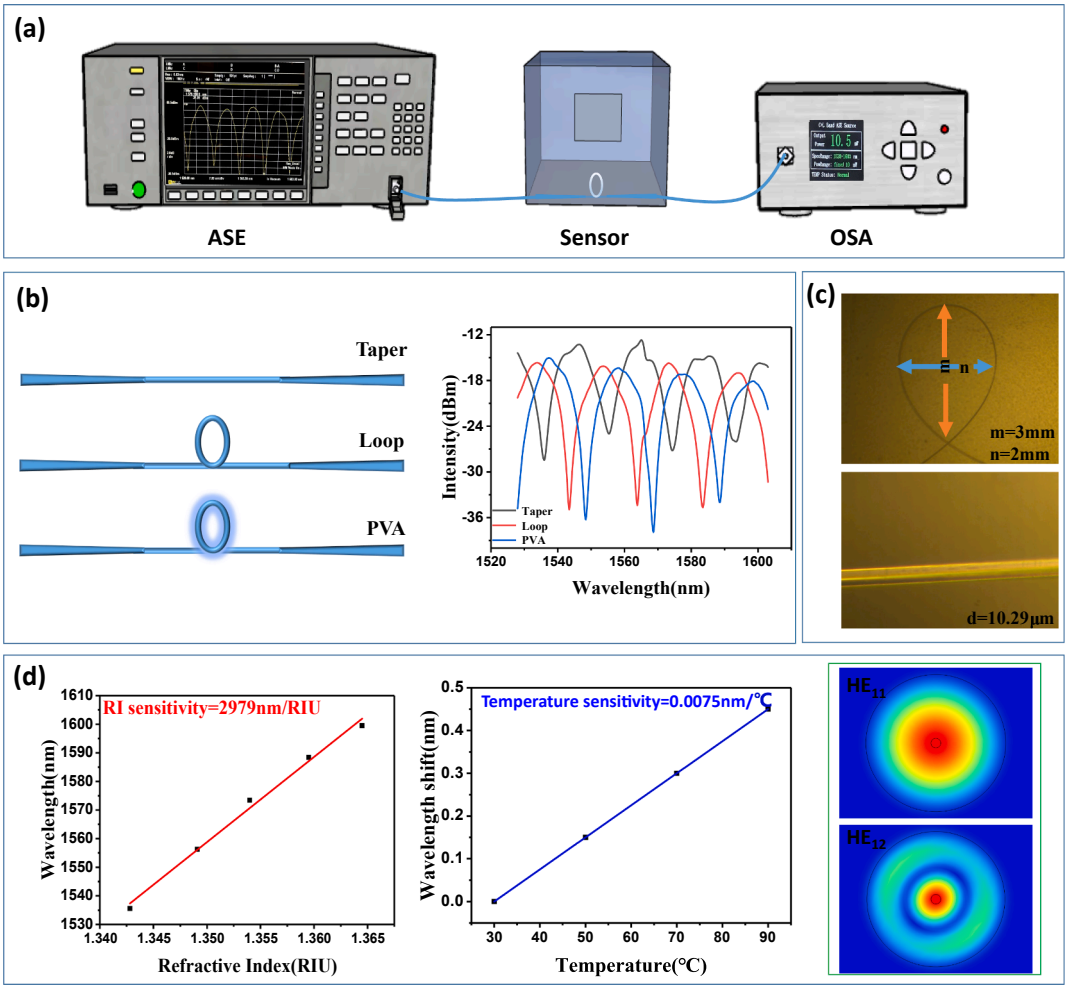

Fig. 1. (a) Schematic diagram of the experiment setup. (b) Making process of the RH sensor structure and the corresponding transmission spectra. (c) Optical micrographs images of the morphology of the sensor. (d) Refractive index, temperature response, and major interferometric modes.

rotators (Thorlabs, HFR007) and placed at a 60° angle. The two rotators are operated in the same direction and at the same speed, so that the microfiber intersects into a loop in the uniform area in Fig. 1 (b, left middle), with the short axis of 2 mm and the long axis of 3 mm as shown in Fig. 1 (c). The loop structure tends to be stable under the clamping apparatus force and electrostatic force, and the spectrum is shown in Fig. 1 (b, right red). PVA solution is mixed with PVA particles (Shanghai Macklin Biochemical Co., Ltd., Poly (vinyl alcohol)105) and deionized water, heating in a water bath by heat-collecting magnetic stirring apparatus (Changzhou Chunqiu electronic instrument Co., Ltd., DF-101S), thus PVA particles are completely dissolved in deionized water to form a uniform 2 %(w/w) PVA solution. 1 %(w/w) solution diluted by deionized water. Finally, the loop region is dipped with PVA solution, which forms a uniform and stable PVA film in Fig. 1 (b, left bottom), and then this region is dried by the heating plate at 60 °C for 10 mins. The final spectrum of the sensor is shown in Fig. 1 (b, right blue).

The RI response of this sensor is recorded from 1.3428 to 1.3645 with wavelength shifted from 1535.55 to 1599.48 nm, with RI sensitivity as high as 2979 nm/RIU and the fitting degree of 0.99043, as shown in Fig. 1 (d, left). Considering that the temperature may affect the experimental results, the analysis of the temperature from 30 to 90 °C is shown that the temperature sensitivity is as low as 0.0075 nm/°C in Fig. 1 (d, middle), which indicating that this sensor has a smaller temperature cross-sensitivity. The numerical analysis (finite analysis software) in Fig. 1 (d, right) shows the electric field modes distribution of HE_{11} and HE_{12} mode.

3.2. RH measurement

The effects of different concentrations of PVA and dip numbers (related to material thickness) on the loop sensor are investigated. The experimental results are shown in Fig. 2. The comparison with the results of dip once and dip twice (1% concentrations of PVA), indicates that the RH response range is the same (40–76 %RH) and the sensitivity of 1 % dip twice (Fig. 2 (b)) can reach 0.533 nm/%RH, which is 3.44 times that of 1 % dip once in Fig. 2 (a) (0.155 nm/%RH). The contrast with the data of 1 % dip twice and 1 % dip three times, the result shows that the sensitivity of 1 % dip twice is lower than that of 1 % dip three times (Fig. 2c) (40–76 %RH), but the RH response range is 2.4 times that of 1 % dip three times (61–76 %RH). Considering the influence of different concentrations on the response range and sensitivity, the PVA concentration is changed to 2 % in the experiment. Compared with the experimental data of 2 % dip once and 1 % dip once, it is found that the RH sensitivity (0.302 nm/%RH) of 2 % dip once (Fig. 2d) is improved, but the RH response interval (51–76 %RH) is significantly reduced. We summarize the experimental results of Fig. 2 in Table 1. Through the comparison of the three groups of experiments, we can conclude that the RH sensor with the optimal parameter (1 % dip twice) has relatively high sensitivity, and the largest RH response range in this experiment is researched. The RH range monitored by the experiment has met the basically thermal comfort conditions of the human body and prevented the corrosion of electronic equipment [36]. The appropriate RH for human body sensation is about is 40 % to 70 %RH [37]. When the RH of

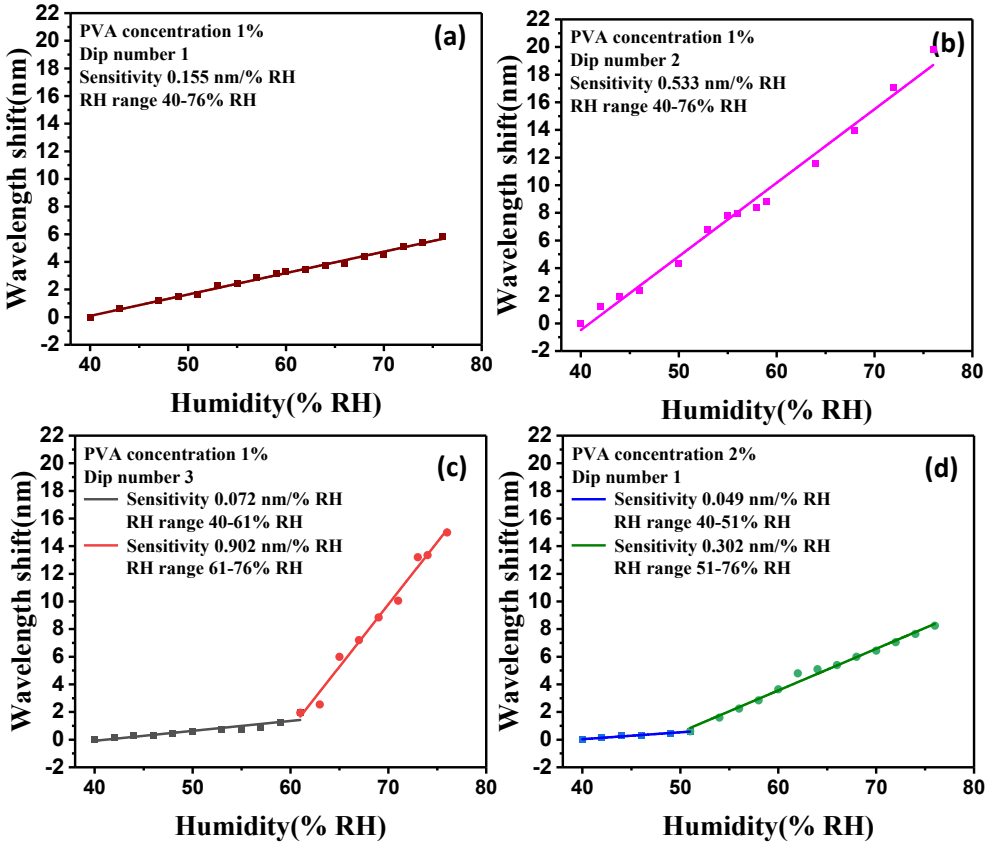

Fig. 2. (a) PVA concentration 1% and dip once with the linear fitting of the wavelength shift. (b) PVA concentration 1% and dip twice with the linear fitting of the wavelength shift. (c) PVA concentration 1% and dip three times with the linear fitting of the wavelength shift. (d) PVA concentration 2% and dip once with the linear fitting of the wavelength shift.

Table 1
RH measurement the results of Fig. 2.

PVA concentration	Dip numbers	RH range (% RH)	Sensitivity (nm/% RH)
1%	1	40–76	0.155
1%	2	40–76	0.533
1%	3	40–61	0.072
		61–76	0.902
2%	1	40–51	0.049
		51–76	0.302

surroundings is equal to or less than 65 %RH, the metal is not easy to corrosion, but more than 65 %RH, the metal could rust even in a clean atmosphere. The laboratory experimental results show that the corrosion critical humidity of iron is 65 %RH, and that of zinc is 70 %RH. Thus, RH monitoring is needed in industrial areas [21]. The proposed sensor in the manuscript can monitor the RH range of 40–76 %RH, which can be used for RH detection critical points (65 % and 70 %RH).

The measured transmission spectra response is shown in Fig. 3 (a) corresponding to Fig. 2 (b) (1 % dip twice). Meanwhile, the intensity variation is shown in Fig. 3 (b), with the intensity response of −0.213 dBm/%RH, as a result of the loss increasing due to adsorption. Fig. 3 (c) depicts that the sensor has a response time of 1.8 s and a recovery time of 4 s. To explore the stability of the sensor, the RH is controlled at a stable value, and the wavelength is recorded for 30 mins with an interval of 5 min in Fig. 3 (d). The results indicate that the wavelength is only small fluctuation, which indicates that the sensor has high stability. Fig. 3 (e) shows the relationship between the wavelength response of the fiber and the RH changes. The hysteresis error is calculated from the experimental results [38,39]. The maximum humidity hysteresis is 8.7 % when the RH is 53 %RH, and the maximum humidity hysteresis is 4.8 % when the RH is 68 %RH. There is a weak hysteresis phenomenon due to external vibrations or slight changes in the environment. Fig. 3 (f) shows the repeated experimental results (three times) of the sensor including standard deviation (s), further confirming the good repeatability of the sensor [40,41]. The formula for calculating the standard deviation is

$$s = \sqrt{\frac{\sum_{i=1}^{r}\left(R_i - \overline{R}\right)^2}{r-1}} \tag{9}$$

where R_i is the wavelength drift of each target measurement result; $\overline{R}$ is the average of wavelength drift, and r is the number of measured data for each concentration. Thus, the standard deviations are calculated with experimental data. Through calculating, the standard deviation is about 0.2 nm indicating that the sensor has good repeatability. Table 2 shows RH sensors based on PVA film with different structures. By comparison, our sensor has good advantages.

4. Conclusion

In this work, we propose and demonstrate the RH sensor based on a loop microfiber modified with PVA film. The experiment results show that the sensor has high RH sensitivity and low-temperature cross-sensitivity. As a sensitized material (PVA), the RH sensor is confirmed that the sensitivity is 0.533 nm/%RH and −0.213 dBm/%RH in the RH range of 40%-76% with the response time of 1.8 s and the recovery time of 4 s. This proposed RH sensor has the advantages of low cost, high sensitivity, good stability, fast response, and easy manufacture, which brings a new platform for RH monitoring in the environment.

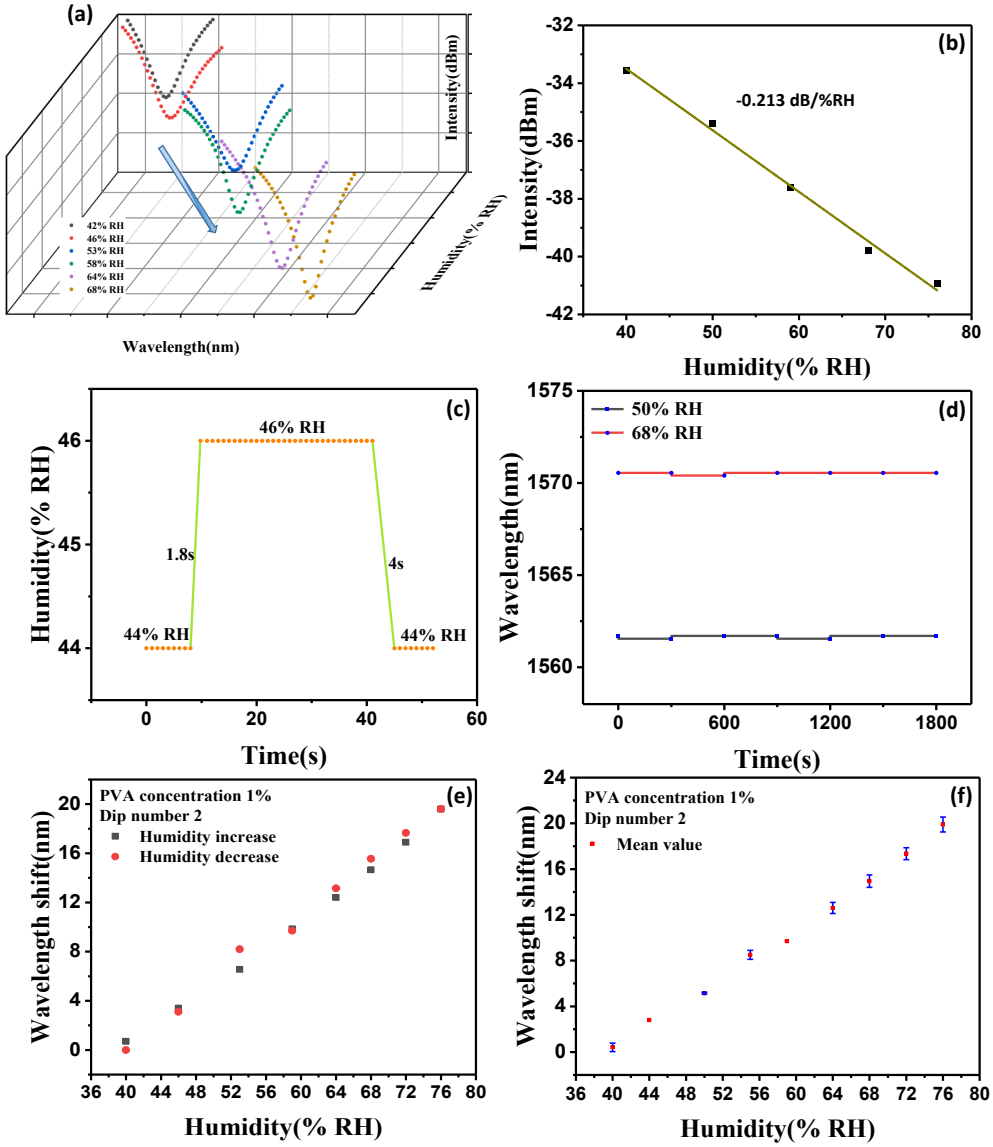

Fig. 3. (a) Transmission spectrum response of the coated loop microfiber under different RH levels. (b) Linear fitting of the intensity modulation. (c) Response time (1.8 s) and recovery time (4 s). (d) Stability test of the proposed sensor. (e) The relationship between the wavelength response of the fiber and the RH changes. (f) The repeated experimental results of the sensor.

Table 2
RH sensors based on PVA film with different structures.

Structure and material	RH sensitivity	Temperature sensitivity	Cost	Manufacturing difficulty	Publication date	Reference
PVA film with an implemented electronic module	−11.5 MHz (60% RH)	medium	medium	difficulty	2000	20
PVA film on a single-mode side-polished fiber	0.53 dB /%RH	low	high	difficulty	2004	21
Knob-integrated fiber Bragg grating with PVA film	1.2 dB/%RH	8.2 pm/°C	high	difficulty	2015	22
Graphene oxide quantum dots and PVA film composite coated tapered no-core fiber combined with a fiber Bragg grating	143.27 pm/% RH	9.21 pm/°C	high	difficulty	2020	24
Spiral micro-structured single mode-multimode-single mode fiber structure with PVA film	650 pm/%RH	medium	high	difficulty	2020	25
No-core multimode interferometer coated with Al_2O_3-PVA composite films	587 pm/%RH	medium	high	difficulty	2020	26
Taper fiber covered with the PVA film	119.4 pm/%RH	29 pm/°C	low	easy	2021	27
Loop microfiber coated with PVA film	533 pm/%RH	7.5 pm/°C	low	easy	2021	this paper

CRediT authorship contribution statement

Dandan Sun: Conceptualization, Methodology, Writing – review & editing, Formal analysis, Funding acquisition. **Jiguang Chen:** Investigation, Data curation, Writing – original draft, Resources. **Yongming Fu:** Validation, Investigation, Formal analysis, Supervision, Funding acquisition. **Jie Ma:** Validation, Investigation, Formal analysis, Supervision, Funding acquisition.

Declaration of Competing Interest

The authors declare that they have no known competing financial interests or personal relationships that could have appeared to influence the work reported in this paper.

Acknowledgments

This work was supported in part by Scientific and Technological Innovation Programs of Higher Education Institutions in Shanxi, China (2019L0084 and 2019L0002), National Natural Science Foundation of China (62005147, 61722507 and 61901249) and Funds for International Cooperation and Exchange of the National Natural Science Foundation of China (62020106014).

References

[1] N. Irawati, H.A. Rahman, H. Ahmad, S.W. Harun, A PMMA microfiber loop resonator-based humidity sensor with ZnO nanorods coating, Measurement 99 (2017) 128–133, https://doi.org/10.1016/j.measurement.2016.12.021.
[2] A. Bahrampour, M. Dehghani Sanij, H. Rooholamininejad, A. Bahrampour, The theoretical study of an optimal distributed fiber moisture sensor based on the periodic polymer coating, Iran, J. Sci. Technol. A Sci. 45 (3) (2021) 1097–1104, https://doi.org/10.1007/s40995-021-01087-3.
[3] J. Li, D.Y. Choi, M. Smietana, Editorial: novel smart materials for optical fiber sensor development, J. Lightwave Technol. 8 (2021), 671086, https://doi.org/10.3389/fmats.2021.671086.
[4] Y. Zhong, Y. Wang, Z. Wang, Z. Xing, Y.i. Xiao, J. Yu, H. Guan, Y. Luo, H. Lu, W. Zhu, Z. Chen, Ultrafast freestanding microfiber humidity sensor based on three-dimensional graphene network cladding, Opt. Express 28 (4) (2020) 4362, https://doi.org/10.1364/OE.379812.
[5] Z. Xu, Z. Li, Dynamic humidity response of surface acoustic wave sensors based on zinc oxide nanoparticles sensitive film, Appl. Phys. A-Mater. 127 (2021) 68–69, https://doi.org/10.1007/s00339-021-04587-6.
[6] J. Tang, Z. Li, M. Xie, Y.u. Zhang, W. Long, S. Long, T. Wen, Z. Fang, W. Zhu, H. Zheng, Y. Luo, H. Guan, H. Lu, J. Zhang, J. Yu, Z. Chen, Optical fiber bio-sensor for phospholipase using liquid crystal, Biosens. Bioelectron. 170 (2020) 112547, https://doi.org/10.1016/j.bios.2020.112547.
[7] S.-C. Tseng, T.-Y. Wu, J.-C. Chou, Y.-H. Liao, C.-H. Lai, J.-S. Chen, S.-J. Yan, M.-S. Huang, T.-W. Tseng, Y.-H. Nien, Research of sensing characteristic and dynamic measurement of graphene oxides modified flexible arrayed RuO_2 chlorine ion sensor, Mater. Res. Bull. 101 (2018) 155–161, https://doi.org/10.1016/j.materresbull.2018.01.015.
[8] K. Zhu, Y. Tang, X. Zhong, L.i. Xiong, Y. Zhang, C. Tan, H. Song, J. Wang, Improved response/recovery time and sensitivity of SnSe nanosheet humidity sensor by LiCl incorporation, Adv. Electron. Mater. 6 (5) (2020) 1901330, https://doi.org/10.1002/aelm.v6.510.1002/aelm.201901330.
[9] H. Farahani, R. Wagiran, G. Urban, MgO-dodped (Zr, Sr)TiO_3 perovskite humidity sensors: microstructural effects on water permeation, Proceedings 1 (4) (2017) 408, https://doi.org/10.3390/proceedings1040408.
[10] C. Zhang, Y. Zhang, K. Cao, Z. Guo, Y. Han, W. Hu, Y. Wu, Y. She, Y. He, Ultrasensitive and reversible room-temperature resistive humidity sensor based on layered two-dimensional titanium carbide, Ceram. Int. 47 (5) (2021) 6463–6469, https://doi.org/10.1016/j.ceramint.2020.10.229.
[11] Z. Xing, Y. Zheng, Z. Yan, Y. Feng, Y.i. Xiao, J. Yu, H. Guan, Y. Luo, Z. Wang, Y. Zhong, Z. Chen, High-sensitivity humidity sensing of microfiber coated with three-dimensional graphene network, Sensor Actuat. B-Chem. 281 (2019) 953–959, https://doi.org/10.1016/j.snb.2018.11.057.
[12] N. Zhou, P. Wang, Z.X. Shi, Y.X. Gao, Y.X. Yang, Y.P. Wang, Y. Xie, D.W. Cai, X. Guo, L. Zhang, J.R. Qiu, L.M. Tong, Au nanorod-coupled microfiber optical humidity sensors, Opt. Express 27 (6) (2019) 8180, https://doi.org/10.1364/OE.27.008180.
[13] B. Troia, D.L. Francesco, M.N. Passaro, Cascaded ring resonator and Mach-Zehnder interferometer with a Sagnac loop for Vernier-effect refractive index sensing, Sensor Actuat. B-Chem. 240 (2017) 76–89, https://doi.org/10.1016/j.snb.2016.08.095.
[14] R. Oliveira, L. Bilro, T.H.R. Marques, C.M.B. Cordeiro, R. Nogueira, Simultaneous detection of humidity and temperature through an adhesive based Fabry-Pérot cavity combined with polymer fiber Bragg grating, Opt. Laser Eng. 114 (2019) 37–43, https://doi.org/10.1016/j.optlaseng.2018.10.007.
[15] G.Y. Chen, X. Wu, C.A. Codemard, L.i. Yu, X. Liu, H. Xu, T.M. Monro, D. G. Lancaster, Optical hygrometer using light-sheet skew-ray probed multimode fiber with polyelectrolyte coating, Sensor Actuat. B-Chem. 296 (2019) 126685, https://doi.org/10.1016/j.snb.2019.126685.
[16] D. Sun, S. Xu, S. Liu, et al., Simultaneous measurement of temperature and relative humidity based on a twist microfiber coated with nanomaterials, Appl. Optics 60 (2021) 3849–3855, https://doi.org/10.1364/AO.423341.
[17] H. Adnan Zain, M. Hafiz Jali, H. Rafis Abdul Rahim, M.d. Ashadi Md Johari, H. Helmi Mohd Yusof, S. Thokchom, M. Yasin, S. Wadi Harun, ZnO nanorods coated microfiber loop resonator for relative humidity sensing, Opt. Fiber Technol. 54 (2020) 102080, https://doi.org/10.1016/j.yofte.2019.102080.
[18] B. Yin, G. Sang, R. Yan, Y. Wu, S. Wu, M. Wang, W. Liu, H. Li, Q. Wang, Wavelength- and intensity-demodulated dual-wavelength fiber laser sensor for simultaneous RH and temperature detection, IEEE Access 8 (2020) 52091–52099, https://doi.org/10.1109/ACCESS.2020.2979470.
[19] E. Maciak, Low-coherence interferometric fiber optic sensor for humidity monitoring based on Nafion® thin film, Sensors 19 (2019) 629, https://doi.org/10.3390/s19030629.
[20] M. Penza, G. Cassano, Relative humidity sensing by PVA-coated dual resonator SAW oscillator, Sensor Actuat. B-Chem. 68 (1-3) (2000) 300–306, https://doi.org/10.1016/S0925-4005(00)00448-2.
[21] G. Ainhoa, P. Fátima, S. Joaquín, Optical fiber relative-humidity sensor with polyvinyl alcohol film, Appl. Optics 43 (2004) 4127–4132, https://doi.org/10.1364/ao.43.004127.
[22] G. Yan, Y. Liang, E.-H. Lee, S. He, Novel Knob-integrated fiber Bragg grating sensor with polyvinyl alcohol coating for simultaneous relative humidity and temperature measurement, Opt. Express 23 (12) (2015) 15624, https://doi.org/10.1364/OE.23.015624.
[23] J. Yeo, Y. Kwon, Humidity sensing performance of defected ground structure-based microwave sensors coated with PMMA, PHEMA, and PVA, Microw. Opt. Techn. Let. 63 (2020) 1194–1200, https://doi.org/10.1002/mop.32746.
[24] Q.-H. Cheng, A.-L. Zhang, H.-G. Pan, W. Li, C.e. Sun, Humidity and temperature sensor based on GOQDs-PVA coated tapered no-core fiber combined with FBG, Optoelectron. Lett. 16 (6) (2020) 428–432, https://doi.org/10.1007/s11801-020-9215-x.
[25] H. Lin, F. Liu, Y. Dai, F. Mumtaz, Relative humidity sensor based on FISM-SMS fiber structure coated with PVA film, Optik 207 (2020) 164320, https://doi.org/10.1016/j.ijleo.2020.164320.
[26] H.Y. Zebian, H.J. Taher, Relative humidity sensor based on no-core multimode interferometer coated with Al_2O_3-PVA composite films, Opt. Fiber Technol. 54 (2020) 102110, https://doi.org/10.1016/j.yofte.2019.102110.
[27] N. Chen, X. Zhou, X. Li, Highly sensitive humidity sensor with low-temperature cross-sensitivity based on a polyvinyl alcohol coating tapered fiber, IEEE T. Instrum. Meas. 70 (2021) 1–8, https://doi.org/10.1109/TIM.1910.1109/TIM.2020.3034154.
[28] D. Sun, L.-P. Sun, T. Guo, B.-O. Guan, Label-free thrombin detection using a tapered fiber-optic interferometric aptasensor, J. Lightwave Technol. 37 (11) (2019) 2756–2761, https://doi.org/10.1109/JLT.5010.1109/JLT.2018.2878762.
[29] Y. Tan, L.-P. Sun, L. Jin, J. Li, B.-O. Guan, Temperature-insensitive humidity sensor based on a silica fiber taper interferometer, IEEE Photonic. Tech. L. 25 (22) (2013) 2201–2204, https://doi.org/10.1109/LPT.2013.2282990.
[30] Y. Peng, Y. Zhao, M.-Q. Chen, F. Xia, Research advances in microfiber humidity sensors, Small 14 (29) (2018) 1800524, https://doi.org/10.1002/smll.201800524.
[31] Y.u. Wu, TianHu Zhang, YunJiang Rao, Y. Gong, Miniature interferometric humidity sensors based on silica/polymer microfiber knot resonators, Sensor Actuat. B-Chem. 155 (1) (2011) 258–263, https://doi.org/10.1016/j.snb.2010.12.030.
[32] S.H. Girei, H.N. Lim, M.Z. Ahmad, M.A. Mahdi, A.R. Md Zain, M.H. Yaacob, High sensitivity microfiber interferometer sensor in aqueous solution, Sensors 20 (17) (2020) 4713, https://doi.org/10.3390/s20174713.
[33] Y. Wang, C. Shen, W. Lou, F. Shentu, C. Zhong, X. Dong, L. Tong, Fiber optic relative humidity sensor based on the tilted fiber Bragg grating coated with graphene oxide, Appl. Phys. Lett. 109 (3) (2016) 031107, https://doi.org/10.1063/1.4959092.
[34] E. Owji, H. Mokhtari, F. Ostovari, B. Darazereshki, N. Shakiba, 2D materials coated on etched optical fibers as humidity sensor, Sci. Rep. 11 (1) (2021), https://doi.org/10.1038/s41598-020-79563-w.
[35] L.P. Sun, T.S. Huang, Z.H. Yuan, et al., Ultra-high sensitivity of dual dispersion turning point taper-based Mach-Zehnder interferometer, Opt. Express 27 (2019) 23103–23111.
[36] M.H. Jali, H.R.A. Rahim, M.A.M. Johari, S.S. Hamid, H.H.M. Yusof, S. Thokchom, P. Wang, S.W. Harun, Optical characterization of different waist diameter on microfiber loop resonator humidity sensor, Sensor Actuat. A-Phys. 285 (2019) 200–209, https://doi.org/10.1016/j.sna.2018.11.025.
[37] E. Traversa, Ceramic sensors for humidity detection: the state-of-the-art and future developments, Sensor Actuat. B-Chem. 23 (2-3) (1995) 135–156, https://doi.org/10.1016/0925-4005(94)01268-M.
[38] M. Hartings, K.O. Douglass, C. Neice, Z. Ahmed, Humidity responsive photonic sensor based on a carboxymethyl cellulose mechanical actuator, Sensor Actuat. B-Chem. 265 (2018) 335–338, https://doi.org/10.1016/j.snb.2018.03.065.

[39] S. Kano, H. Mekaru, Nonporous inorganic nanoparticle-based humidity sensor: evaluation of humidity hysteresis and response time, Sensors 20 (2020) 3858, https://doi.org/10.3390/s20143858.
[40] L. Liang, L. Jin, Y. Ran, L.-P. Sun, B.-O. Guan, Fiber light-coupled optofluidic waveguide (FLOW) immunosensor for highly sensitive detection of p53 protein, Anal. Chem. 90 (18) (2018) 10851–10857, https://doi.org/10.1021/acs.analchem.8b02123.
[41] H. Zhang, Z. Jia, X. Lv, J. Zhou, L. Chen, R. Liu, J.i. Ma, Porous silicon optical microcavity biosensor on silicon-on-insulator wafer for sensitive DNA detection, Biosens. Bioelectron. 44 (2013) 89–94, https://doi.org/10.1016/j.bios.2013.01.012.